

Spatial and Temporal Evolutions of Dressed Photon Energy Transfer

M. Ohtsu^{1,2}, T. Kawazoe³, H. Saigo⁴

¹ Institute of Engineering Innovation, Graduate School of Engineering,
The University of Tokyo, 2-11-16 Yayoi, Bunkyo-ku, Tokyo, 113-8656, Japan

² Research Origin for Dressed Photon,
c/o The University of Tokyo, 2-11-16 Yayoi, Bunkyo-ku, Tokyo, 113-8656, Japan

³ Tokyo Denki University,
Tokyo Senju Campus, Bldg.4-9F 906A, Senju-Asahi-cho, Adachi-ku, Tokyo 120-8551, Japan

⁴ Nagahama Institute of Bio-Science and Technology,
1266 Tamura-cho, Nagahama-shi, Shiga, 526-0829, Japan

Abstract: It has been shown that dressed photon (DP) energy transfer exhibits unique autonomous spatial evolution features, and novel functional devices have been demonstrated as a first example of the practical application of this transfer. Temporal evolution features originating from nutating DP energy transfer followed by radiative relaxation have also been demonstrated. A novel film for highly efficient optical energy conversion is presented as a second example of the application of these features. It is suggested that these spatial and temporal evolution features can be analyzed based on theoretical models based on a quantum walk and a random walk. This film was placed on a silicon solar battery to convert UV light energy to visible light energy, resulting in an increased electrical power generation efficiency of 20.2%.

1 Introduction

The dressed photon (DP) is a novel form of quantum field, which is created in a nanometer-sized space [1]. It is also called an off-shell photon because it exists in the off-shell area that is displaced from the shell of the dispersion relation between energy and momentum. In drawing a physical picture of this quantum field, there have been some problems originating from the intrinsic nature of the DP; namely, its electromagnetic mode could not be defined do to its sub-wavelength size. However, recently developed novel

theories have succeeded in solving these problems, allowing the intrinsic properties of the DP to be suitably described. These properties are:

- (a) A DP is created in or on the surface of a nano-particle (NP).
- (b) The created DP localizes on the NP, and the extent of localization is equivalent to the size of the NP.

Two novel phenomena were predicted as a result of successfully describing these properties. They are:

- (1) A transition that is normally electric dipole-forbidden becomes allowed.
- (2) Size-dependent resonance occurs.

These phenomena, which originate from DP energy transfer between NPs, have been experimentally confirmed and applied to the development of a variety of novel application technologies. Progress in this area has been reviewed in a previous article in the Off-shell Archive [2].

Section 2 of the present paper reviews unique features of DP energy transfer between NPs, based on phenomena (1) and (2) above. Section 3 introduces the principles and practices of novel nanometric functional devices and an optical energy converter. Section 4 reviews the application of this DP energy transfer to optical energy conversion. In Sections 3 and 4, spatial and temporal evolutions of the DP energy transfer are demonstrated. A summary and conclusions are presented in Section 5.

2 Energy transfer of dressed photons

Novel devices that operate by using DPs are named DP devices. Some of these devices are introduced in Section 3. In order to examine the principle of operation of DP devices, two different-sized cubic semiconductor NPs are assumed, in which exciton energy is quantized, as schematically explained by Fig. 1. Small and large NPs (NP_S and NP_L , respectively) in this figure are used as input and output terminals, respectively. These NPs are irradiated with propagating light whose photon energy is resonant with the lowest quantized energy level (1,1,1) of the exciton in NP_S . This light corresponds to the input signal to the DP device. The propagating light emitted from the lowest energy level (1,1,1) in the large NP_L corresponds to the output signal.

Based on the localized nature of the DP (property (1) in Section 1), these NPs are installed in close proximity to each other, with a separation as short as their sizes. By assuming that the ratio between their side lengths is

$1:\sqrt{2}$, one can readily find that the exciton energy of level (1,1,1) in NP_S is equal to that of level (2,1,1) in NP_L ; that is, these two energy levels are resonant with each other. It should be noted that level (2,1,1) in NP_L is an electric-dipole forbidden level, whereas level (1,1,1) in NP_S is an electric-dipole allowed level. Thus, the energy of the irradiated propagating light normally cannot be transferred from level (1,1,1) in NP_S to level (2,1,1) in NP_L .

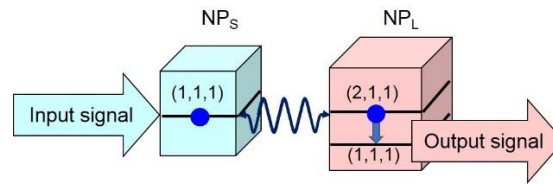


Fig. 1

DP energy transfer and dissipation in two cubic semiconductor NPs.

However, because of phenomena (1) mentioned above in Section 1, there is a way for the energy to be transferred from NP_S to NP_L , as represented by the blue double-headed arrow in Fig. 1. The transfer process is:

- (1) An exciton is excited to level (1,1,1) in NP_S by the irradiated propagating light.
- (2) A DP is created by this exciton and is localized on NP_S .
- (3) The energy of this DP is transferred to NP_L .
- (4) An exciton is excited to level (2,1,1) in NP_L even though this level is electric-dipole forbidden.

After this process, the exciton promptly relaxes to the lower level (1,1,1) in the NP_L and dissipates a small amount of energy, as shown by the downward blue arrow. Then, the relaxed exciton emits propagating light, to be used as the output signal.

3 Application to functional devices

The unique transfer and dissipation of the DP energy, reviewed in the previous section, have been applied to the development a variety of novel DP devices, such as AND and NOT logic gates, by integrating size-controlled

semiconductor NPs on a substrate. Figure 2 demonstrates the structure and operation of these devices [3]. In addition to these logic gate devices, a variety of other DP devices have been developed, including a nano-optical condenser [4], a digital-to-analog converter [5], an energy transmitter [6], a frequency up-converter [7], a delayed-feedback optical pulse generator [8], and so on. As representative examples of these devices, this section reviews a nano-optical condenser and an energy transmitter.

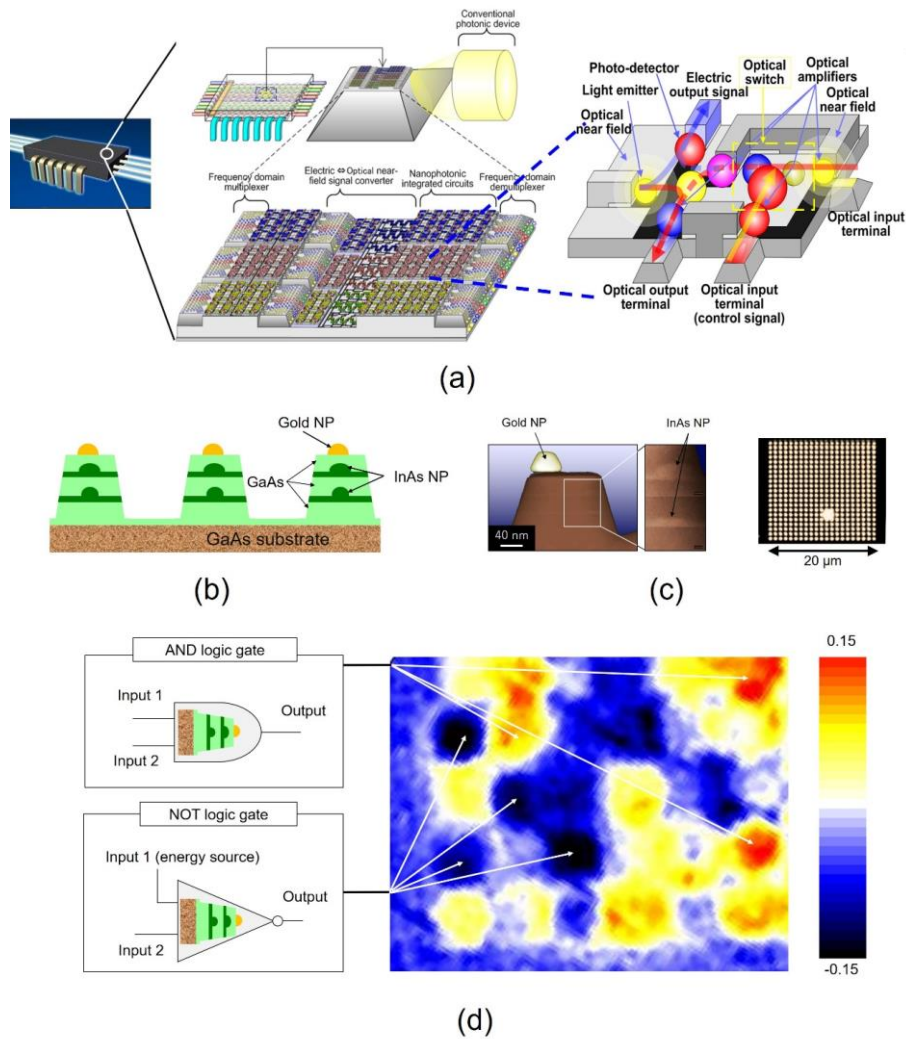


Fig. 2 Dressed photon devices.

(a) Prototype of integrated circuit composed of DP devices.

(b) Cross-sectional structure of mesa-shaped NOT logic gate composed of InAs NPs.

(c) Scanning transmission electron microscope image of structure in (b) (left) and optical microscope image of a two-dimensional array of structures in (b) (right).

(d) Measured spatial distribution of the output signal intensity from a two-dimensional array of fabricated devices composed of InAs NPs.

3.1 Nano-optical condenser

A nano-optical condenser that converts propagating light to DPs with high efficiency has been developed on the basis on the unique spatial evolution features of the DP energy transfer [4]. In order to construct this device, a large number of small nano-particles (NP_S) are used, and one large nano-particle (NP_L) is installed at the center, as shown in Fig. 3(a). Moreover, medium-sized nano-particles (NP_M) are installed in the intervening spaces. Since the sizes of these NPs are tuned so that the quantized exciton energy levels are resonant with each other, as was the case between the two NPs in Fig. 1, when an exciton is created in NP_S by irradiation with propagating light, the DP energy is transferred from NP_S to NP_M . After this transfer, relaxation promptly occurs in NP_M , and subsequently, the energy is transferred from NP_M to NP_L . After relaxation in NP_L , the output signal is generated from the exciton in the lowest energy level. Here, since the energy level (1,1,1) in NP_S is tuned to the photon energy of the incident propagating light, almost all the incident propagating light energy can be absorbed by a large number of NP_S .

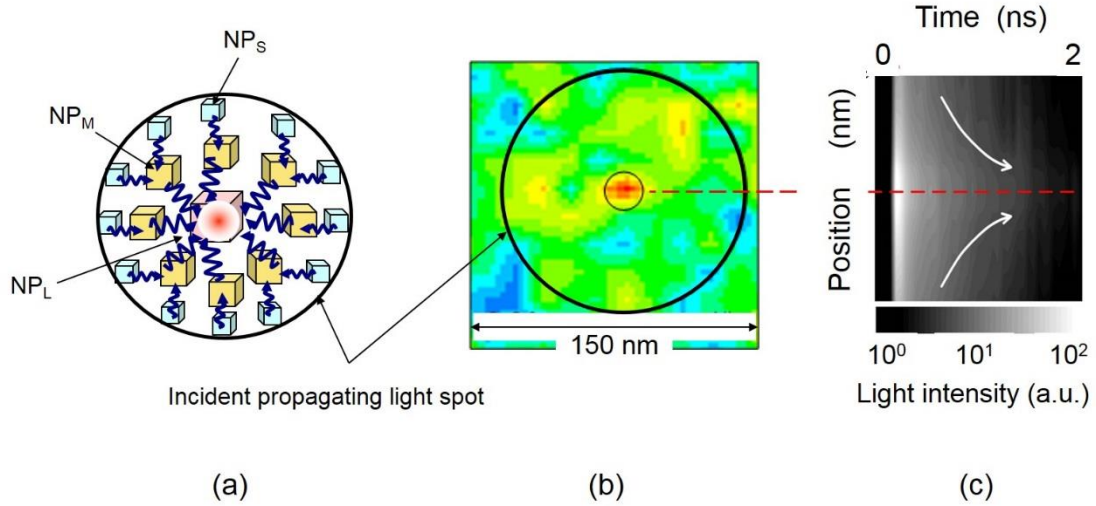


Fig. 3 Nano-optical condenser.

(a) Structure of the device. (b) and (c) show the spatial distribution and temporal evolution of the light intensity emitted from CuCl NPs, respectively.

Furthermore, since the energy dissipation in this system is due to the relaxation in NP_M and NP_L , its magnitude is very small. As a result, a high

efficiency is expected for concentrating the energy of the incident propagating light at NP_L .

Figure 3(b) shows an observed near field optical microscopic image of the spatial distribution of the DP energy by applying propagating light with a wavelength of 385 nm to cubic CuCl NPs in an NaCl host crystal. The bright spot at the center corresponds to the place at which the incident light energy was condensed at NP_L , which had a side length of 8 nm. Its diameter was about 20 nm, including the size of the probe apex used for the microscope, which governs the resolution of the measurement. The light power in this spot was more than five-times higher than that of the light power emitted from NP_L when it was isolated from the NPs. From these results, it is confirmed that this device worked as a high-efficiency optical condenser beyond the diffraction limit. This novel device has also been called an optical nano-fountain [4].

The high performance of this device can be confirmed by comparing it with a conventional convex lens. When propagating light is focused by a convex lens, the theoretical spot diameter at the focal plane is expressed as λ / NA , which corresponds to the diffraction limit of a focused light beam. Here, λ is the wavelength of the incident light, and NA is a parameter called the numerical aperture, which depends on the shape and material of the lens, being smaller than unity. By substituting the spot diameter in Fig. 3(b) into this formula, we find that NA is more than 40, which is much larger than that of a conventional convex lens.

Figure 3(c) shows the measured spatial and temporal evolutions of the light intensity. The horizontal axis at the top of the figure represents time, and the vertical axis represents the radial position in polar coordinates centered at NP_L . The brightness gradation is proportional to the number of emitted photons, from which one can find that the energy is condensed at NP_L with a time constant as short as 2 ps.

Because of the extremely low energy dissipation due to the relaxation from the upper to lower energy levels in NP_M and NP_L , the efficiency of optical energy concentration can be higher than 0.9. The energy transfer process in the nano-optical condenser described above is similar to that in photosynthetic bacteria [9], whose high energy transfer efficiency is receiving attention as a novel system function inherent to such complex systems in a nano-scale space [10,11].

3.2 Energy transmitter

In addition to the nano-optical condenser described above, another example that uses the spatial evolution features of the DP energy transfer is an energy transmitter. This transmitter is used to transmit a signal from one DP device to another, corresponding to the function of a metallic wire in an electrical circuit or an optical waveguide in a conventional optical integrated circuit. It should meet the following two requirements:

- (1) Signal reflection from the DP devices connected to the tail of this transmitter must be avoided to achieve stable uni-directional energy transmission.
- (2) Transmission loss must be sufficiently low to realize a long transmission length.

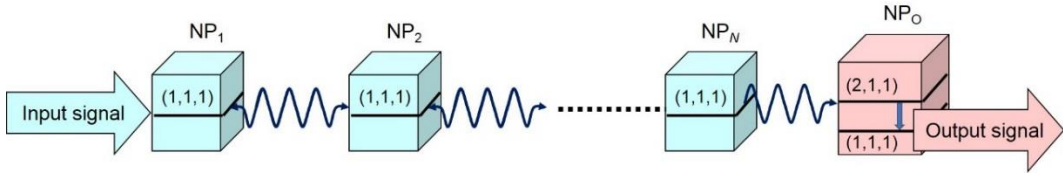


Fig. 4 Structure of energy transmitter.

Figure 4 shows the structure of an energy transmitter that was developed to meet these requirements. It is composed of an array of N NPs of the same size ($NP_1 - NP_N$), and a large NP (NP_O) installed at the end of this array. In the case of using cubic NPs, as an example, an exciton is created in energy level $(1,1,1)$ in NP_1 by applying an input signal, i.e., by irradiating NP_1 with propagating light. This light is converted to a DP and is transferred to energy level $(1,1,1)$ in NP_N , and nutation occurs among the N NPs. As a result, these NPs are coupled with each other. If the size of NP_O is tuned so that its electric dipole-forbidden level $(2,1,1)$ is resonant with the energy level of this coupled state of the N NPs, nutating energy is transferred to the upper energy level $(2,1,1)$ in NP_O , and by subsequent relaxation to the lower energy level $(1,1,1)$. Finally, the light is emitted from the exciton in level $(1,1,1)$ and is used as the output signal.

The device in Fig. 4 meets requirement (1) above because the exciton cannot be excited to the upper energy level $(2,1,1)$ in NP_O even if the exciton is created in the lower energy level $(1,1,1)$ in NP_O by back-transfer of

the signal from the DP devices installed at the stage after NP_0 . Thus, the energy is not back-transferred from NP_0 to $NP_1 - NP_N$.

It can be easily found that requirement (2) is met because the magnitude of the energy dissipated during the relaxation from level (2,1,1) to level (1,1,1) in NP_0 is as low as 20 meV, which is much lower than the photon energy of the light radiated onto the device.

For device fabrication, it is much easier to randomly disperse $NP_1 - NP_N$ and NP_0 on a substrate than to arrange them accurately so as to maintain a constant separation. Figure 5(a) schematically explains this configuration [12], in which small NPs are randomly dispersed along the x -, y -, and z -axes, and are used as $NP_1 - NP_N$, whose numbers of rows are denoted by N_x , N_y , and N_z , respectively. NP_0 is installed among the dispersed small NPs. NP_1 and NP_0 are respectively denoted by NP_{in} and NP_{out} in this figure.

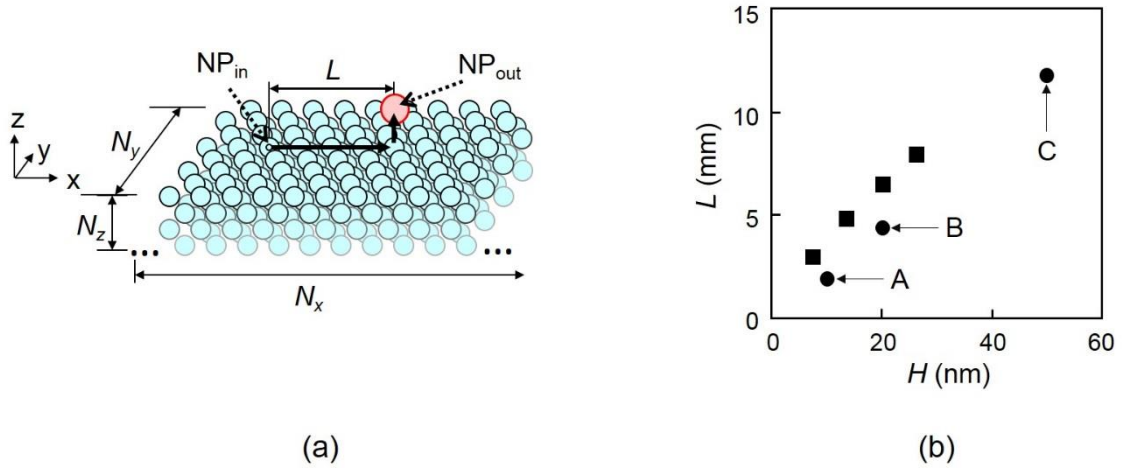


Fig. 5 Calculated results for NPs dispersed on a planar substrate.

(a) Arrangement of multiple small NPs (NPs) and one larger NP (NP_L).

(b) Dependence of the energy transfer length L on the thickness H of the small NP layers.

For experiments, spherical CdSe NPs were used for simplicity of material preparation. The diameters of $NP_1 - NP_N$ were maintained at 2.8 nm, whereas that of NP_0 was 4.1 nm in order to satisfy the resonance condition of the exciton energy levels. These spherical CdSe NPs were dispersed on a SiO_2 substrate, and the average separation between the

adjacent NPs was arranged to be close to 7.3 nm in order allow efficient DP energy transfer (refer to property (b) in Section 1). Moreover, the thickness of the NP layers, H in Fig. 5(a), was fixed to 10 nm, 20 nm, and 50 nm, which is proportional to the number of rows N_z of $\text{NP}_1 - \text{NP}_N$ along the z -axis. These devices are denoted by A, B, and C, respectively.

By applying propagating light with a wavelength of 473 nm, the energy transfer length L was measured as a function of H . The results are shown in Fig. 5(b), from which the values of L for devices A, B, and C were found to be 1.92 μm , 4.40 μm , and 11.8 μm , respectively. These are much longer than the wavelength of the incident light, which also meets requirement (2) above. This figure shows that these measured values agree with the values calculated by using the rate equations representing DP energy transfer between two adjacent NPs. It also shows that L increases with increasing H , i.e., with increasing N_z .

3.3 Autonomy in dressed photon energy transfer

The DP devices reviewed in the previous subsections exhibit novel characteristics which are superior to those of conventional photonic devices. They are: single-photon operation [13], low energy dissipation [14], low energy consumption [15], tamper resistance [16], and skew resistance [17]. Furthermore, an outstanding advantage conferred by the spatial evolution features is autonomy in the DP energy transfer [18], which is reviewed in this subsection.

As is schematically explained by Fig. 6(a), the present model contains N small NPs (NP_S) and one large NP (NP_L). By assuming that each NP_S is initially occupied by an exciton, quantum master equations for the density matrix are solved to derive the occupation probability of the exciton in the lower energy level in NP_L . The time-integrated value of this probability corresponds to the output signal intensity.

This intensity is calculated as a function of the number N of CuSe NP_S . The calculated results are indicated by closed circles in Fig. 6(b) and show that the efficiency in energy transfer is highest when $N \cong 4$. Since the radiative relaxation rate from the lower energy level in NP_L takes a finite value, the DP energy is not transferred to NP_L until the exciton in the lower energy level is annihilated, and as a result, the energy is dissipated from

NP_S if N is too large. Therefore, the output signal intensity does not increase if too many NP_S are installed around an NP_L , and as a result, the efficiency of the energy transfer to NP_L decreases when N is larger than 4.

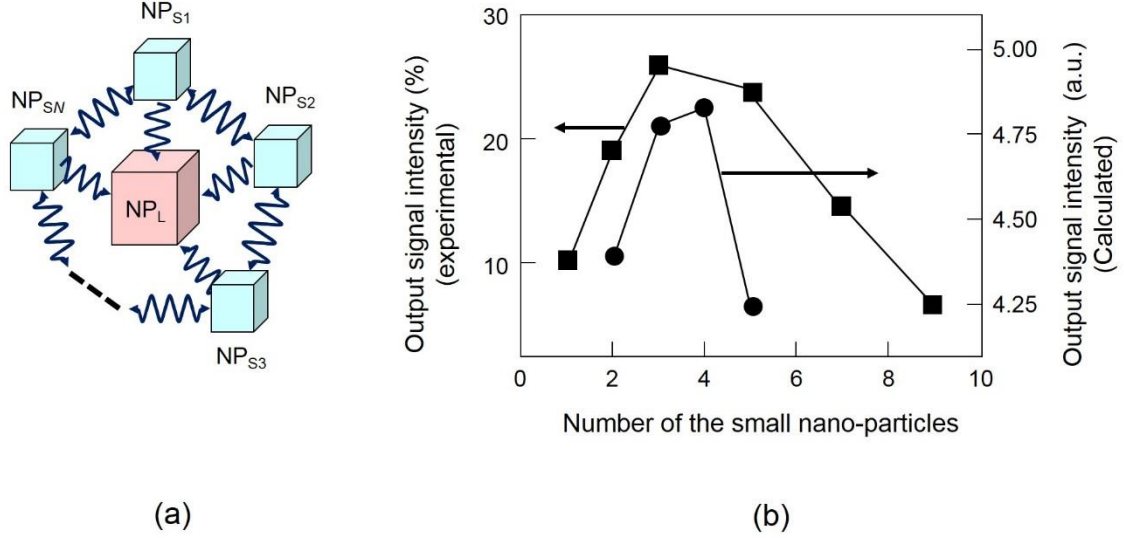


Fig. 6 Autonomy of the DP energy transfer.

(a) Layout of NPs. (b) Dependences of the output signal intensities emitted from CuSe NPs on the ratio of the number of NP_S s to that of NP_L .

Small and large spherical CdSe NPs (2.0 nm and 2.8 nm diameters, respectively) were used, as was the case described in Subsection 3.2, to experimentally measure the magnitude of the energy transferred from NP_S to NP_L . The results are represented by the closed squares in Fig. 6(b), which show that the output signal intensity takes the maximum at $N \cong 4$.

The dependence of the energy transfer on the number N of the NPs suggests that the output signal intensity can be controlled by designing the positions of the NPs. Let us assume that interactions between some NP_S s and NP_L may be degraded or lost because their resonant conditions are not satisfied due to, for example, size-detuning of NPs, fluctuations in the separations between NPs, and deterioration of the NP materials. In the case of a pentagonal layout, as shown in Fig. 7(a), there can be eight degraded configurations: By referring to system E0 without any degradations, system E1 represents the layout in which the interaction between one NP_S and NP_L is degraded or lost (represented by the mark \times between NP_{S1} and NP_L in this figure). Systems E2 and E2' have two degraded interactions.

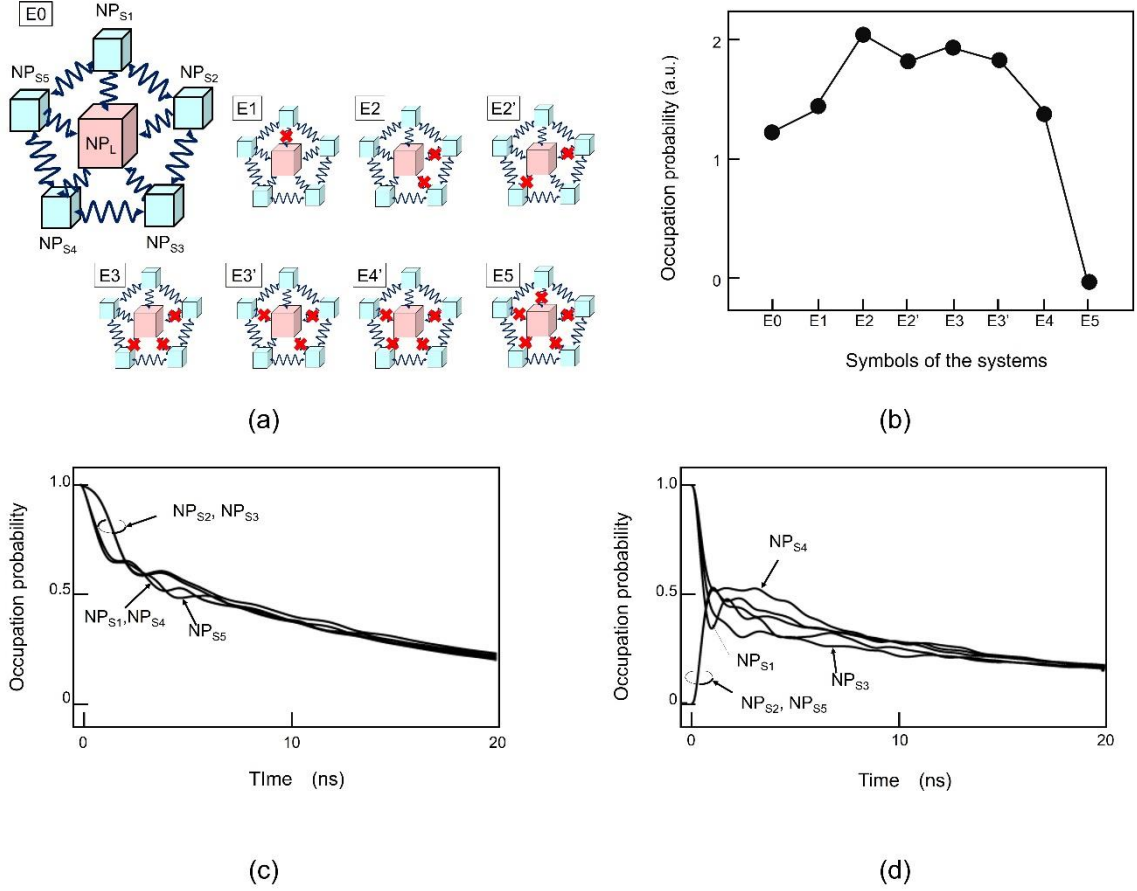


Fig. 7 Degraded or lost interaction between NP_{SS} and NP_L .

(a) Layout of NPs. (b) Time-integrated values of the occupation probabilities for systems E0 to E5. (c) and (d) are temporal evolutions of the occupation probabilities of the exciton in the energy levels in five NP_{SS} in systems E2 and E0, respectively.

Figure 7(b) shows the relation between the systems (E0–E5) and the time-integrated values of the occupation probability of the exciton in NP_L . This figure shows that system E5 does not generate any output signals because the interaction between NP_S and NP_L is completely lost. In contrast, the output signal intensities from systems E1–E4 with degraded interactions are larger than that from system E0. In particular, the value of the output signal intensity from system E2 is 1.64-times that from system E0, which is consistent with the fact that the signal intensity takes the maximum at $N \cong 4$ in Fig. 6(b).

Moreover, the autonomy in energy transfer can be understood from Fig. 7(c). This figure shows the temporal evolutions of the occupation

probabilities of excitons in the energy levels in five NP_S in system E2, in which two interactions are degraded ($\text{NP}_{S2}\text{-NP}_L$ and $\text{NP}_{S3}\text{-NP}_L$), as was shown in Fig. 7(a). The energy levels in all the NP_S are initially occupied by excitons, and afterward for several ns, the occupation probabilities in NP_{S2} and NP_{S3} remain high, which means that the energy is efficiently stored in NP_{S2} and NP_{S3} until it is transferred to NP_L . On the other hand, Fig. 7(d) shows the time evolutions of the occupation probabilities in the case of system E0, in which the energy levels in three NP_S (NP_{S1} , NP_{S3} , and NP_{S4}) are initially occupied by excitons. It is found from this figure that the occupation probabilities for NP_{S2} and NP_{S5} increased within 2 ns even though they were initially zero. This means that, in a sense, the transferred energy autonomously searches for unoccupied NP_S s in the system.

It was demonstrated that a single energy transfer process is about 10^4 -times more efficient compared with the single bit-flip energy required in conventional electronic devices [14]. On the other hand, energy transfer in light harvesting antennas exhibits superior efficiency [19], and these structures have similarities to nanostructures networked via interactions by DP energy transfer. In summary, these studies will be extremely helpful for developing advanced DP devices with higher performance.

3.4 Temporal evolution of dressed photon energy transfer

In addition to the spatial evolutions shown in Subsections 3.2 and 3.3, Fig. 8 (a) shows the temporal evolution of the output signal from the DP device, i.e., the light intensity from NP_L , emitted when a propagating light pulse (pulse width: 10 ps) is applied to NP_S . Red circles are the measured values acquired for $0 \leq t \leq 4$ ns. The optical intensity increases rapidly with a rise time τ_r of 90 ps, which depends on the magnitude of the transferred DP energy. After the applied signal pulse decays, the output signal also decays with small amplitude oscillation. This oscillation originates from the nutation of the DP energy transfer between NP_S and NP_L . The period of oscillation is found to be about 400 ps from this figure. The decay time, i.e., the fall time τ_f , is about 4 ns, which depends on the value of the radiative relaxation rate from the low energy level in NP_L . The solid curve represents the result calculated by using quantum master equations for the density matrix [20], which agrees

well with the experimental results.

For more detailed analyses of the temporal evolution of the DP energy transfer, the optical intensity was acquired in the time range $0 \leq t \leq 10$ ns, which is longer than that in Fig. 8(a). Black squares in Fig. 8(b) are the acquired values. The blue curve represents the temporal evolution expressed as $\exp(-t/\tau_{f1})$, where τ_{f1} is the fall time, depending on the magnitude of the transferred DP energy. This curve agrees with the black squares only for an initial stage as short as $0 \leq t \leq 2$ ns. On the other hand, the red curve represents the temporal evolution expressed as $\exp(-\sqrt{t/\tau_{f2}})$, where the fall time τ_{f2} is the radiative relaxation rate from the low energy level in NPL. This agrees with the black squares for a wide range of time periods up to 10 ns. For more detailed analyses of the DP energy transfer dynamics, it will be advantageous to suppress the component expressed as $\exp(-\sqrt{t/\tau_{f2}})$, which can be realized by decreasing the device temperature.

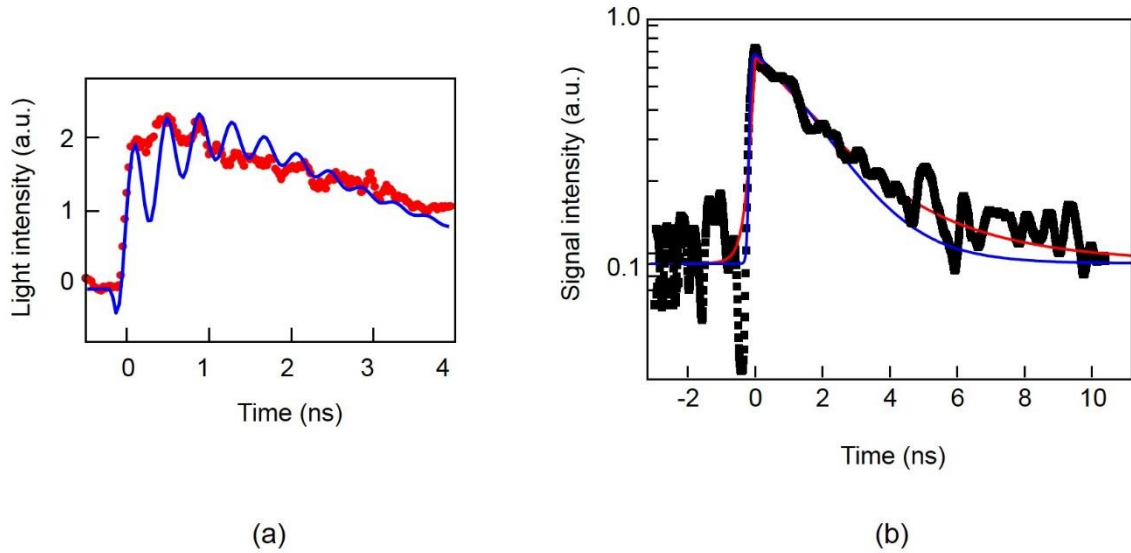


Fig. 8 Temporal evolution of the light intensity emitted from the CuCl NPL.

(a) and (b) are the optical intensities, acquired for $0 \leq t \leq 4$ ns and for $0 \leq t \leq 10$ ns, respectively.

4 Application to optical energy conversion

A novel thin film was invented recently, which efficiently converts ultraviolet (UV) photon energy to visible photon energy by means of DP energy transfer and dissipation. It has been used to drastically improve the electrical power generation efficiency of a solar cell battery. This section reviews the principle and operation of this film.

4.1 Principle

Transparent silicone or ethylene-vinyl acetate (EVA) was used as the film material, with a thickness of $10\ \mu\text{m}$. ZnO semiconductor NPs (average size and number density are 3–5 nm and 10^{17} to $10^{18}/\text{cm}^3$, respectively) and DCM dye NPs (weight density 3–5 mg/cm^3) were dispersed in this film. It is required that the separation between the ZnO and DCM NPs be as close as possible to their sizes in order to transfer the DP energy between them (refer to (b) in Section 1). The number density and weight density above meet this requirement [21,22].

The roles of the ZnO and DCM NPs in this film are to absorb UV light and emit visible light, respectively. They correspond respectively to NP_S and NP_L in Fig. 1. That is, UV light absorption excites an electron in the ZnO NP to create the DP. Then, the DP energy is transferred to the DCM NP, resulting in excitation of the electron in the DCM NP. This electron dissipates a small amount of its energy by relaxing to a lower energy level, emitting visible light.

For the DP energy transfer, an electronic dipole-forbidden transition is utilized (refer to (1) in Section 1). Furthermore, since the magnitude of the energy dissipation above is very low, very high-efficiency optical energy conversion can be realized.

Figures 9(a) and (b) show the electronic energy levels in the ZnO and DCM NPs for UV light absorption and visible light emission, respectively. They are:

[In ZnO NP]

$|a_{\text{ZnO}}\rangle$: An energy level of the electron in the conduction band. Since it is an electric dipole-allowed level, the electron is excited to this level by UV light absorption.

$|a'_{\text{ZnO}}\rangle$: An electric dipole-allowed energy level in the conduction band. Its energy is slightly lower than that of $|a_{\text{ZnO}}\rangle$.

$|b_{\text{ZnO}}\rangle$: Several energy levels in the bandgap, which originate from impurity atoms in the ZnO NP. They consist of electric dipole-allowed and -forbidden energy levels.

$|c_{\text{ZnO}}\rangle$: An electric dipole-allowed level of the energy levels $|b_{\text{ZnO}}\rangle$ above, which is a defect level originating from the oxygen atoms in the ZnO NP. The electron in this level emits blue light.

$|e_{\text{ZnO}}\rangle$: An electric dipole-forbidden level of the energy levels $|b_{\text{ZnO}}\rangle$ above.

However, it can emit light because it is the lowest energy level of $|b_{\text{ZnO}}\rangle$.

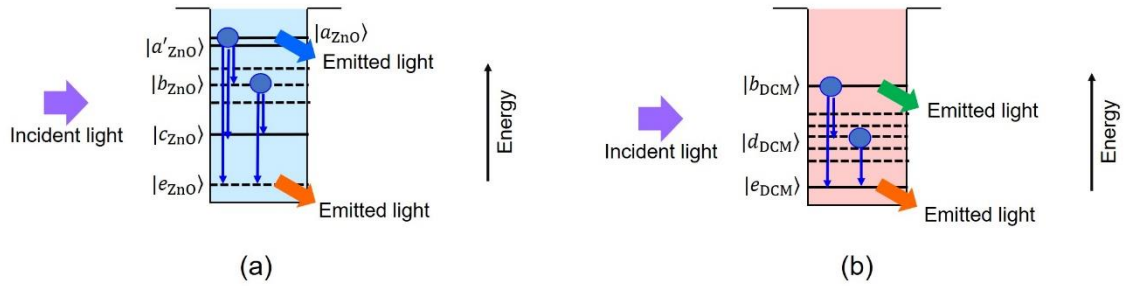


Fig. 9 Electronic energy levels in a ZnO NP (a) and a DCM NP (b).

[In DCM NP]

$|b_{\text{DCM}}\rangle$: An electric dipole-allowed level. Thus, the electron in this level can emit light. It is resonant with the energy level $|b_{\text{ZnO}}\rangle$ in the ZnO NP.

$|d_{\text{DCM}}\rangle$: Electric dipole-forbidden energy levels, which originate from the impurity atoms in the DCM NP. Some of them are resonant with the energy level $|c_{\text{ZnO}}\rangle$ in the ZnO NP.

$|e_{\text{DCM}}\rangle$: An electric dipole-allowed level of the energy levels $|d_{\text{DCM}}\rangle$. Thus, the electron in this level can emit light. It is resonant with the energy level $|e_{\text{ZnO}}\rangle$ in the ZnO NP.

The UV light absorption and visible light emission processes in the ZnO NP and DCM NP, are:

[In ZnO NP (Fig. 9(a))]

An electron in the ZnO NP is excited to the energy level $|a_{\text{ZnO}}\rangle$ by UV light absorption. This excited electron has a higher probability of UV light emission than that of relaxation to a lower energy level. Thus, the conversion efficiency from UV light to visible light is low.

[In DCM NP (Fig. 9(b))].

After an electron in the DCM NP is excited to a higher energy level by UV light absorption, it relaxes to an electric dipole-forbidden energy level, which is a triplet energy level. Thus, the conversion efficiency from UV light to visible light is low.

However, in the case where both the ZnO and DCM NPs are dispersed in the film, the light absorption and emission processes are remarkably different from those above. They are (Fig. 10): An electron in the ZnO NP is excited to the energy level $|a_{\text{ZnO}}\rangle$ by UV light absorption. It subsequently relaxes to the lower energy levels $|b_{\text{ZnO}}\rangle$, $|c_{\text{ZnO}}\rangle$, or $|e_{\text{ZnO}}\rangle$. Then, a DP is created, and its energy is transferred to the resonant energy levels $|b_{\text{DCM}}\rangle$, $|d_{\text{DCM}}\rangle$, or $|e_{\text{DCM}}\rangle$ in the DCM NP. As a result, an electron is excited to these levels and emits visible light. This visible light emission realizes a high efficiency of energy conversion from UV light to visible light. It should be noted that the DP energy can be transferred back from the DCM to the ZnO particles even though the electron in the DCM particles relaxes to the triplet energy level. This back transfer contributes to further increases in the energy conversion efficiency.

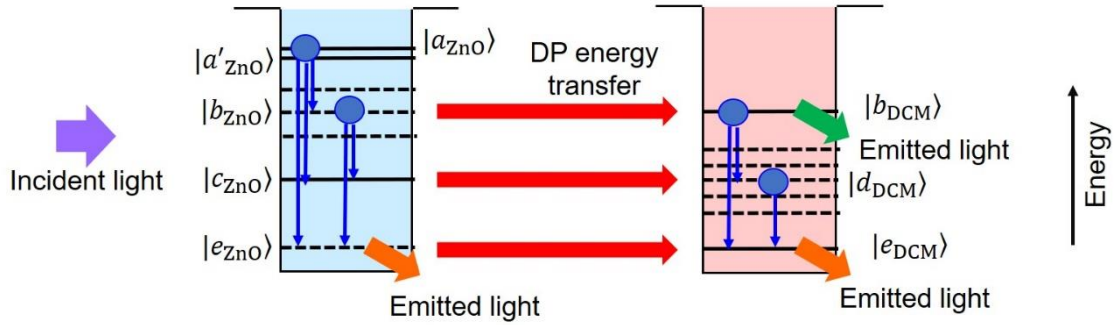


Fig. 10 Light absorption and emission of a film in which ZnO and DCM NPs are dispersed.

4.2 Operating characteristics

Figure 11 shows measured excitation spectra, in which the horizontal axis represents the wavelength of the light incident on the film, and the vertical axis is the intensity of the visible light (wavelength 560 nm) emitted from the electron in the energy level $|e_{\text{DCM}}\rangle$ of the DCM NP. Figures 11(a) and (b) show the results acquired when only the ZnO and DCM NPs are dispersed in the film, respectively. Figure 11(c) shows those when both ZnO and DCM NPs are dispersed. Comparing the areas below the curves in these figures, the efficiency of the conversion from UV light to visible light (wavelength 560 nm) energy in Fig. 11(c) is estimated to be at least 10-times higher than that in Fig. 11(a) or (b).

Furthermore, a bump A on the curve in Fig. 11(c) represents that the efficiency of the visible light emission is selectively enhanced when the incident UV light is resonant with the energy level $|a_{\text{ZnO}}\rangle$ of the ZnO NP. Furthermore, the bumps B and C also represent that the efficiency is selectively enhanced when the incident light is resonant with the energy level $|b_{\text{ZnO}}\rangle$ or $|c_{\text{ZnO}}\rangle$ of the ZnO NP. These selective enhances are due to the DP energy transfer to the energy levels $|b_{\text{DCM}}\rangle$ or $|d_{\text{DCM}}\rangle$ of the DCM NPs, and subsequent relaxation to the energy level $|e_{\text{DCM}}\rangle$.

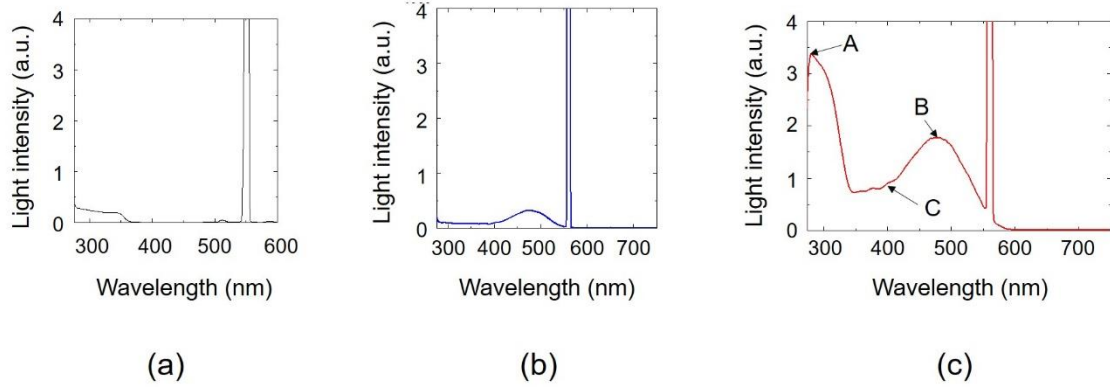


Fig. 11 Excitation spectra.

(a) and (b) The results acquired when only the ZnO and DCM particles are dispersed in the film, respectively. (c) The result when both ZnO and DCM particles are dispersed.

Figure 12 shows the measured relation between the incident UV light intensity (wavelength 325 nm) and the efficiency of the energy conversion to visible light (wavelength 560 nm). It shows that the measured efficiency is proportional to the square of the incident UV light intensity*. This is because the conversion efficiency is proportional to the product of the numbers of DPs created in the ZnO and DCM NPs.

* Figure 12 shows that the efficiency saturates when the UV light intensity is higher than 0.2 W/m². Since the UV light component in sunlight is higher than 0.2 W/cm², this saturation is advantageous for the solar cell battery application to be reviewed in Section 4.3 because the conversion efficiency is maintained constant even if the incident sunlight intensity may vary from hour to hour during daytime.

Figure 13 shows the temporal evolution of the light intensity emitted from the film when a propagating light pulse (pulse width: 2 ps) was applied to the NPs. Figures 13(a) and (b) were acquired when only the ZnO and DCM NPs were respectively dispersed in the film. They are nothing more than the intensities of the light emitted from the ZnO and DCM NPs, respectively, as a result of conventional fluorescence.

The rise time τ_r of the light intensity is as short as 10 ps in Fig. 13(a) and (b). On the other hand, the fall time τ_f is as long as 15 ns and 1.4 ns, respectively, which corresponds to the radiative relaxation rate.

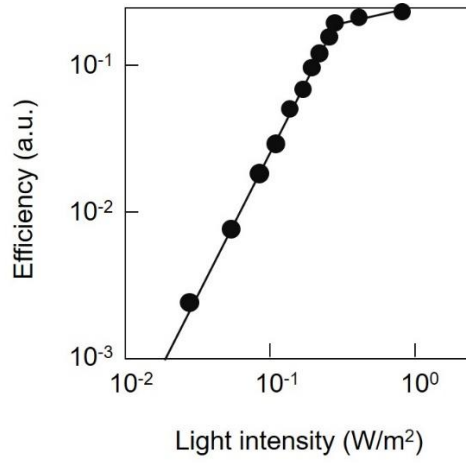


Fig. 12 Measured relation between the incident UV light intensity (wavelength 325 nm) and the efficiency of the energy conversion.

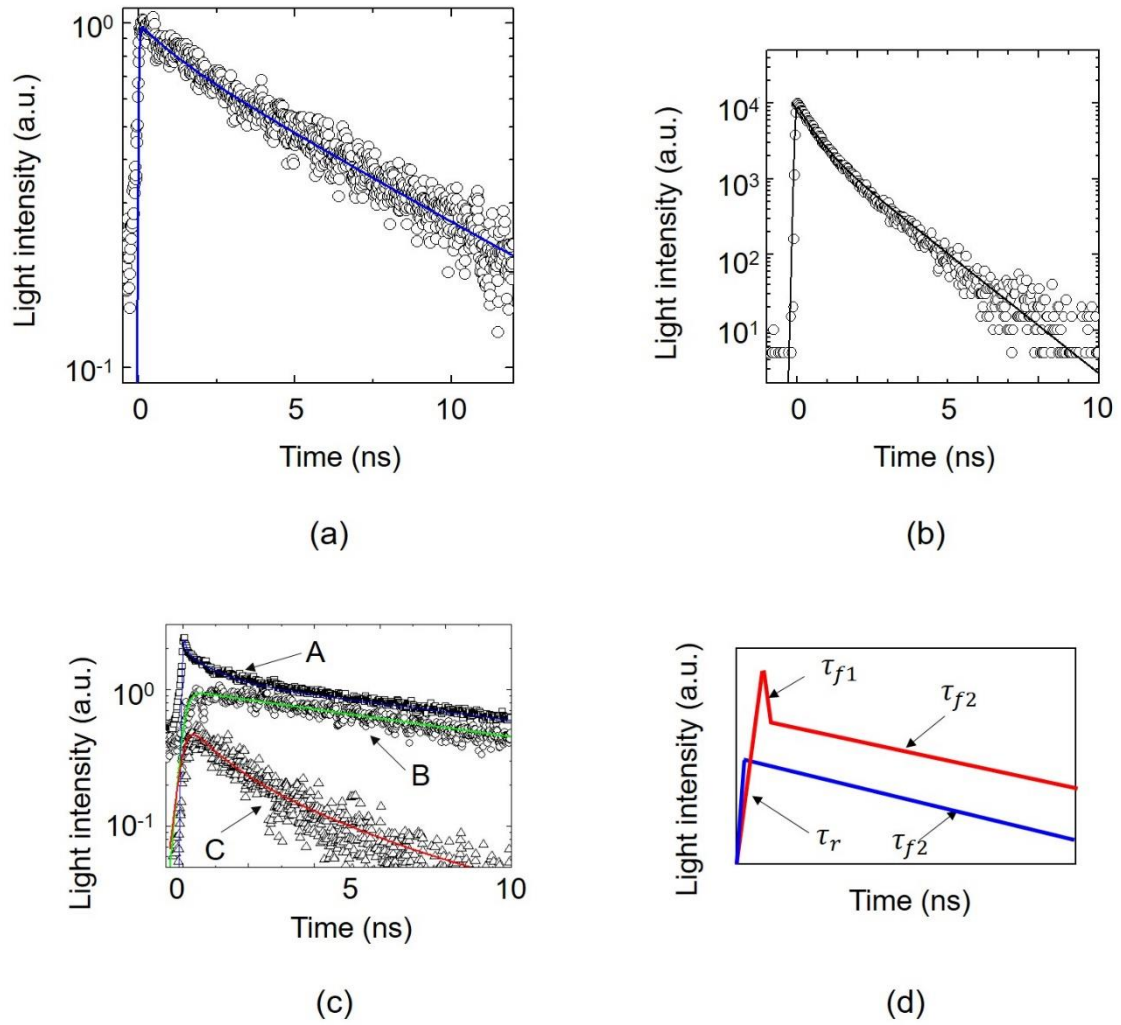


Fig. 13 Temporal evolutions of the light intensity emitted from the film.

(a) The result acquired when only the ZnO NPs are dispersed in the film. The vertical axis represents the light intensity (wavelength 350 nm) emitted from the electron in the lower energy level $|a'_{\text{ZnO}}\rangle$ of the ZnO by illuminating the film with light (wavelength 340 nm), which is resonant with the higher energy level $|a_{\text{ZnO}}\rangle$.

(b) The result acquired when only the DCM NPs are dispersed in the film. The vertical axis represents the light intensity (wavelength 560 nm) emitted from the electron in the energy level $|e_{\text{DCM}}\rangle$ of the DCM by illuminating the film with light (wavelength 340 nm).

(c) The result acquired when both the ZnO and DCM NPs are dispersed in the film. Curve A represents the light intensity (wavelength 350 nm) emitted from the electron in the lower energy level $|a'_{\text{ZnO}}\rangle$ of the ZnO by illuminating the film with light (wavelength 340 nm), which is resonant with the energy level $|a_{\text{ZnO}}\rangle$.

Curve B represents the light intensity (wavelength 560 nm) emitted from the electron in the energy level $|e_{\text{DCM}}\rangle$ of the DCM by illuminating the film with light (wavelength 340 nm), which is resonant with the energy level $|a_{\text{ZnO}}\rangle$ in the ZnO.

Curve C represents the light intensity (wavelength 420 nm) emitted from the electron in the energy levels $|b_{\text{ZnO}}\rangle$ and $|d_{\text{DCM}}\rangle$ of the ZnO and DCM, respectively, by illuminating the film with light (wavelength 420 nm), which is resonant with the energy level $|c_{\text{ZnO}}\rangle$ in the ZnO. (d) Schematic explanation of the curves in (c).

Figure 13(c) shows the results acquired when both ZnO and DCM NPs are dispersed in the film. Figure 13(d) is a schematic explanation of the curves in Fig. 13(c). The time constant τ_r in this figure represents the rise time. Two constants τ_{f1} and τ_{f2} represent two different fall times. Figure 13(c) shows that the values of τ_r and τ_{f1} are 100–150 ps. These correspond to the DP energy transfer times from the ZnO to DCM NPs, which are much

longer than the fluorescence rise times in Figs. 13(a) and (b).

Similar to the fall time of the curves in Figs. 13(a) and (b), the fall time τ_{f2} is 15 ns, which is much longer than τ_{f1} . This fall time τ_{f2} corresponds to the value of the radiative relaxation rate. It means that, after the DP energy transfer, conventional fluorescence occurs in the case where both the ZnO and DCM NPs are dispersed in the film. It should be noted that Figs. 13(a) and (b) do not have the temporal behaviors represented by the time constants τ_r and τ_{f1} .

The temporal evolutions shown in Figs. 8 and 13(c) have several common features even though the materials used are different:

- (1) The temporal evolution expressed as $\exp(-t/\tau_{f1})$ and the nutation behavior in Fig. 8 have the same origin as that of the time evolution represented by τ_{f1} in Fig. 13(c), namely, the DP energy transfer between NPs. The rise time τ_r also originates from this transfer.
- (2) The temporal evolution expressed as $\exp(-\sqrt{t/\tau_{f2}})$ in Fig. 8 has the same origin as that of the time evolution represented by τ_{f2} in Fig. 13(c), namely, the radiative relaxation in each NP.

Features (1) and (2) above represent unique phenomena which are different from each other. The former is exactly the novel off-shell scientific phenomenon [2]. The latter is no more than a conventional on-shell phenomenon. The fact that these temporal evolutions are respectively expressed as $\exp(-t/\tau_{f1})$ and $\exp(-\sqrt{t/\tau_{f2}})$ suggests that they correspond to the quantum walk [23] and the relaxation processes, respectively. As for the former process, it should not be considered as a mere random walk because its energy transportation is linearly dependent on time, not on the square root of time. It is expected that the unique autonomous spatial evolution feature described in Subsection 3.3 can be also analyzed in terms of a quantum walk, one fundamental feature of which is a linear dependence on time.

4.3 Evaluation of the optical energy conversion efficiency

It is expected that the optical energy conversion efficiency of the film is as high as 90%–95% by referring to the large difference between the DP energy transfer time ($\tau_r, \tau_{f1} = 100\text{--}150$ ps) and the lifetime ($\tau_{f2} = 15$ ns) for fluorescent light emission from the DCM NP. Based on this expectation, a novel film was fabricated for converting UV light energy (wavelength 300–350 nm) to visible light energy (wavelength 560 nm) by dispersing ZnO and DCM NPs (Fig. 14(a)) [24]. By putting this film on the surface of a commercially available Si solar cell battery (surface area $156\text{ mm} \times 156\text{ mm}$, nominal electrical power generation efficiency 18.1 %), the electrical power generation efficiency was measured to be as high as 20.0 %, which is an increase of 1.9 % compared with the nominal efficiency mentioned above.

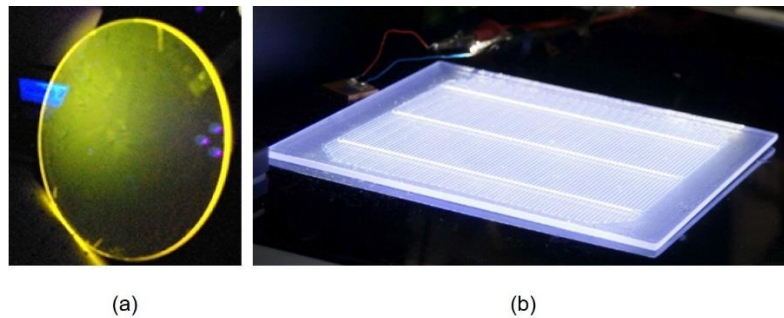


Fig. 14 Photographic images of the film.

The film is $10\ \mu\text{m}$ thick and is coated on the front surface of a glass substrate. After an index-matching oil is coated on the rear surface, it is placed on a solar cell battery surface.

(a) ZnO and DCM NPs are dispersed in the film. (b) ZnO and BBQ NPs are dispersed in the film.

To realize an even higher increase, another type of film was recently developed by replacing the DCM NPs with BBQ dye NPs (Fig. 14(b)), which allowed UV light in the wavelength range 300–350 nm to be efficiently converted to visible light with a wavelength of 450 nm [25]. By putting this film on the surface of the Si solar battery above, the electrical power generation efficiency was measured to be as high as 20.2 %, which is an increase of 2.1 % compared with the nominal efficiency mentioned above.

It should be pointed out that the efficiencies higher than 20% realized by these films have never been achieved with conventional solitary Si solar batteries. The technical details of the method of fabricating these films will be published elsewhere.

5. Summary

The introduction of this paper reviewed the intrinsic nature of the DP, which is a novel form of quantum field created in a nanometer-sized space. Next, a unique DP energy transfer process between semiconductor nanoparticles was described. As a first application of this transfer, novel functional devices were demonstrated by focusing on a nano-optical condenser and an energy transmitter. It was shown that the DP energy transfer in these devices exhibited an autonomous spatial evolution feature. A temporal evolution feature was also demonstrated, which originated from nutating DP energy transfer followed by radiative relaxation.

As a second application, a highly efficient optical energy conversion film was demonstrated. By evaluating the temporal evolution feature of the converted optical energy, the origin of this feature was confirmed to be equivalent to that of the functional devices described above. It was suggested that the spatial and temporal evolutions above can be analyzed based on theoretical models involving a quantum walk and a random walk. As an application of this film, it was placed on a silicon solar battery to convert UV light energy to visible light energy, resulting in an increased electrical power generation efficiency of 20.2%.

References

- [1] M. Ohtsu: *Dressed Photons* (Springer, Heidelberg, 2014) pp.11-37.
- [2] M. Ohtsu, Offshell: 1709R.001.v1 (2019).
- [3] T. Kawazoe, M. Ohtsu, S. Aso, Y. Sawado, Y. Hosoda, K. Yoshizawa, K. Akahane, N. Yamamoto, M. Naruse, Appl. Phys. B **103**, 537 (2011).
- [4] T. Kawazoe, K. Kobayashi, M. Ohtsu, Appl. Phys. Lett. **86**, 103102 (2005).
- [5] M. Naruse, T. Miyazaki, F. Kubota, T. Kawazoe, K. Kobayashi, S. Sangu, and M. Ohtsu, Opt. Lett. **30**, 201 (2005).
- [6] W. Nomura, T. Yatsui, T. Kawazoe, M. Ohtsu, J. Nanophotonics **1**, 011591 (2007).
- [7] T. Yatsui, S. Sangu, K. Kobayashi, T. Kawazoe, M. Ohtsu, J. Yoo, G.-C. Yi, Appl. Phys.

Lett. **94**, 083113(2009).

[8] M. Naruse, H. Hori, K. Kobayashi, T. Kawazoe, M. Ohtsu, Appl. Phys.B **102**, 717(2011).

[9] H. Imahori, J. Phys. Chem. B **108**,6130 (2004).

[10] M. Naruse, T. Kawazoe, R. Ohta, W. Nomura, M. Ohtsu, Phys. Rev. B **80**, 125325 (2009).

[11] N. Johnson, *Simply Complexity*, (Oneworld Publications, Oxford, 2007).

[12] W. Nomura, T. Yatsui, T. Kawazoe, M. Naruse, M. Ohtsu, Appl. Phys.B **100**, 181 (2010).

[13] T. Kawazoe, S. Tanaka, M. Ohtsu, J. Nanophotonics **2**, 029502 (2008).

[14] L.B. Kish, IEE Proc. Circ. Dev. Syst. **151**, 190 (2004).

[15] M. Naruse, P. Holmstrom, T. Kawazoe, K. Akahane, N. Yamamoto, L. Thylen, M. Ohtsu, Appl. Phys. Lett. **100**, 241102 (2012).

[16] M. Naruse, H. Hori, K. Kobayashi, M. Ohtsu, Opt. Lett. **32**,1761 (2007).

[17] M. Naruse, F. Pepper, K. Akahane, N. Yamamoto, T. Kawazoe, N. Tate, M. Ohtsu, ACM J. on Emerging Technol. in Computing Systems **8**, 4-1 (2012).

[18] M. Naruse, K. Leibnitz, F. Peper, N. Tate, W. Nomura, T. Kawazoe, M. Murata, M. Ohtsu, Nano Commun. Networks **2**,189 (2011).

[19] A. Olaya-Castro, C.F. Lee, F.F. Olsen, N.F. Johnson, Phys. Rev. B **78**, 085115 (2008).

[20] S. Sangu, K. Kobayashi, T. Kawazoe, A. Shojiguchi, M. Ohtsu, Trans. Materials Res. Soc. Jpn. **28**, 1035 (2003).

[21] T. Kawazoe, A. Mizushima, K. Matsue, and M. Ohtsu: "A wavelength conversion film using energy transfer via dressed photon," Abstract of the 60th JSAP Spring Meeting, March 2013, Atsugi, Japan, paper number 28p-A1-11.

[22] T. Kawazoe, K. Matsue, and M. Ohtsu: "Fabrication of ZnO-QDs for wavelength conversion film using a dressed photon," Abstract of the 74th JSAP Autumn Meeting, September 2013, Kyoto, Japan, paper number 18p-C14-16.

[23] N. Konno, *Quantum Walk*, Chapter 8, Quantum Potential Theory, ed. by U. Franz and M. Schürmann, (Springer, Heidelberg, 2008) pp.309-452.

[24] T. Kawazoe, K. Matsue, and M. Ohtsu: "Size control of ZnO quantum dots in a wavelength conversion film using a dressed photon for a solar cell," Abstract of the 61st JSAP Spring Meeting, March 2014, Sagamihara, Japan, paper number 18a-F12-6.

[25] T. Kawazoe, C. Amagai, and M. Ohtsu: "High-effectiveness of crystalline silicon solar cell by a wavelength conversion film using a dressed photon," Abstract of the 62th JSAP Spring Meeting, March 2015, Hiratsuka, Japan, paper number 11p-A12-7.